1-1-2020

Position Control of a 3D Printed Soft Finger with Integrated Soft Pneumatic Sensing Chambers

Charbel Tawk
charbel@uow.edu.au

Emre Sariyildiz
University of Wollongong, emre@uow.edu.au

Hao Zhou
University of Wollongong, hzhou@uow.edu.au

Marc in het Panhuis
University of Wollongong, panhuis@uow.edu.au

Geoffrey M. Spinks
University of Wollongong, gspinks@uow.edu.au

See next page for additional authors

Position Control of a 3D Printed Soft Finger with Integrated Soft Pneumatic Sensing Chambers

Abstract

© 2020 IEEE. Soft robots require robust soft and flexible sensors that can undergo large deformations repeatedly. This work reports on soft robotic fingers with embedded soft pneumatic sensing chambers that are directly 3D printed without requiring postprocessing. A low-cost and open-source fused deposition modeling (FDM) 3D printer that employs an off-the-shelf soft thermoplastic poly(urethane) (TPU) was used to fabricate the monolithic fingers and sensing chambers. These pneumatic sensing chambers have multiple advantages including very fast response to any change in their internal volume, linearity, negligible hysteresis, repeatability, reliability, stability over time, long lifetime and very low power consumption. The performance of these chambers is accurately predicted, and their topologies are optimized using finite element modeling (FEM). Also, the flexion of the soft robotic finger is predicted using a geometric model for use in real-time position control. The position control of the soft robotic finger is achieved using feedback signals from the soft pneumatic sensing chambers embedded in the finger.

Disciplines

Engineering | Physical Sciences and Mathematics

Publication Details

Tawk, C., Sariyildiz, E., Zhou, H., in het Panhuis, P., Spinks, G. & Alici, G. (2020). Position Control of a 3D Printed Soft Finger with Integrated Soft Pneumatic Sensing Chambers. 2020 3rd IEEE International Conference on Soft Robotics, RoboSoft 2020 (pp. 446-451). United States: IEEE.

Authors

Charbel Tawk, Emre Sariyildiz, Hao Zhou, Marc in het Panhuis, Geoffrey M. Spinks, and Gursel Alici

Effects of Carbon Content on the Electrochemical Performances of MoS_2-C Nanocomposites for Li-Ion Batteries

Weiyi Sun[a], Zhe Hu[b], Caiyun Wang[c], Zhanliang Tao[a,b,*], Shu-Lei Chou[b,*], Yong-Mook Kang[d,*], Hua-Kun Liu[b]

[a.] Key Laboratory of Advanced Energy Materials Chemistry (Ministry of Education), College of Chemistry; Nankai University, Tianjin 300071, China *Email: taozhl@nankai.edu.cn.

[b.] Institute for Superconducting and Electronic Materials, Australian Institute of Innovative Materials, University of Wollongong, Innovation Campus, Squires Way, North Wollongong, NSW 2500, Australia.*Email: shulei@uow.edu.au.

[c.] ARC Centre of Excellence for Electromaterials Science, Intelligent Polymer Research Institute, University of Wollongong, Squires Way, North Wollongong, NSW 2500, Australia

[d.] Department of Energy and Materials Engineering, Dongguk University-Seoul, Seoul, 100-715, Republic of Korea. *E-mail: dake1234@dongguk.edu.

KEYWORDS: Li-ion batteries, MoS_2, anode, effect of carbon content, stability

ABSTRACT: Molybdenum disulfide is popular for rechargeable batteries, especially in Li-ion batteries, due to its layered structure and relatively high specific capacity. In this paper, we report MoS_2-C nanocomposites which are synthesized by a hydrothermal process, and their use as anode material for Li-ion batteries. Ascorbic acid is used as

the carbon source, and the carbon contents can be tuned from 2.5wt% to 16.2wt%. With increasing of carbon content, the morphology of MoS_2-C nanocomposites changes from nanoflowers to nanospheres, and the particle size is decreased from 200nm to 60nm. This change is caused by the chemical complex interaction of ascorbic acid. The MoS_2-C nanocomposite with 8.4 wt% C features a high capacity of 970 $mAh \cdot g^{-1}$ and sustains a capacity retention ratio of nearly 100% after 100 cycles. When the current increases to 1000 $mA \cdot g^{-1}$, the capacity still reaches 730 $mAh \cdot g^{-1}$. The above manifests that the carbon coating layer does not only accelerates the charge transfer kinetics to supply quick discharging and charging, but also holds the integrity of the electrode materials as evidenced by the long cycling stability. Therefore, MoS_2-based nanocomposites could be used as commercial anode materials in Li-ion batteries.

1. INTRODUCTION

Among the different kinds of devices for energy storage and conversion, lithium ion batteries (LIBs) are considered to be important to people's daily lives because of their characteristics of relative safety, portability, and long life.[1-4] Nevertheless, commercial graphite anode suffers from low specific capacity of 372 mAh g^{-1}.[5-6] For purpose of increasing the capacity and maintain long run-time in portable devices, various kinds of anode materials having the predominance of high capacity are being researched.[7-10] Recently MoS_2, a transition metal dichalcogenide compound, has attracted intensive attention for energy storage,[11-14] owing to its high specific capacity and unique large interlayer spacing which provides two-dimensional diffusion channel for Li^+. MoS_2 as a conversion-type anode material features a high theoretical capacity of 670 $mAh \cdot g^{-1}$. The process of Li^+ ion intercalation forming the intermediate Li_xMoS_2, and then converting to the Mo metal and Li_2S are basic for the electrochemical

reaction of Li-MoS_2 batteries.[15-17] The reaction brings large volume changes and introduces a serious problem of high irreversible capacity which is ascribed to the separation of the Mo metal and Li_2S matrix.[18] In addition, the conductivity of MoS_2 is not high, which limits its rate performance. Since Li-MoS_2 batteries were first reported by Haering et al.,[19] many forms of nanostructured MoS_2 have been investigated to solve the above problems.[16, 20-23] Ultrasmall, single-layer MoS_2 nanoplates decorated with carbon nanofibers (38wt%) were made by electrospinning in Maier's group.[20] Xu and co-workers synthesized MoS_2-C via a simple hydrothermal method, with carbon content approximately 10 wt%, and achieved a high capacity of 888.1 and 511 $mAh \cdot g^{-1}$ at a current density of 100 and 1000 $mA \cdot g^{-1}$, respectively.[23] Liu et al. synthesized expanded layers in MoS_2-graphene nanocomposites by using butyllithium,[24] and they demonstrated a stable capacity of ~1300 $mAh \cdot g^{-1}$ after 200 cycles at 100 mA g^{-1}. All such reports show that modification of nanostructured MoS_2 with carbon materials is a very efficient method to accelerate the speed of the ionic and electronic transport.[17, 22, 24-27] In summary, control of the MoS_2 particle size and the carbon content in the composite (as little as possible) is very necessary.

Although many carbon materials have been tried for loading MoS_2, studies on the effects of the carbon content on the electronic and ionic transport, as well as the electrochemical performance, are limited. Herein we have synthesized MoS_2-C nanocomposites with expanded interlayer spacing through an ascorbic acid assisted hydrothermal method. The carbon source is ascorbic acid, which as an additive for refining the particle size. The as-prepared MoS_2-C with a carbon content of 8.4wt% exhibits a considerable capacity of 970 $mAh \cdot g^{-1}$ at 100 mA g^{-1} and 730 $mAh \cdot g^{-1}$ at 1000 mA g^{-1}. After 100 cycles at 100 mA g^{-1}, the discharge capacity is still as high as 970 $mAh \cdot g^{-1}$, with capacity retention of 97.3%.

2. EXPERIMENTAL SECTION

The MoS_2 and MoS_2-C samples preparing by the hydrothermal method were shown in Fig. 1.[28] Briefly, 0.3 g $Na_2MoO_4 \cdot 2H_2O$ and 0.4 g $CS(NH_2)_2$ were

dissolved in 30 mL of distilled water. The designed amount of ascorbic acid was added, and by the addition of concentrated hydrochloric acid (HCl), the pH was adjusted to 1. After stirring for 30 min, the precursors were transferred into a 45 mL Teflon-lined stainless steel autoclave and maintained at 180 °C for 24 h. The resultant black precipitate was centrifuged and washed with distilled water and ethanol. After drying in a vacuum oven and annealing at 700°C for 3 h, the final products were obtained. The molar ratios of $Na_2MoO_4 \cdot 2H_2O$ to ascorbic acid for the different samples were 2:0, 2:1, 2:2, and 2:3.

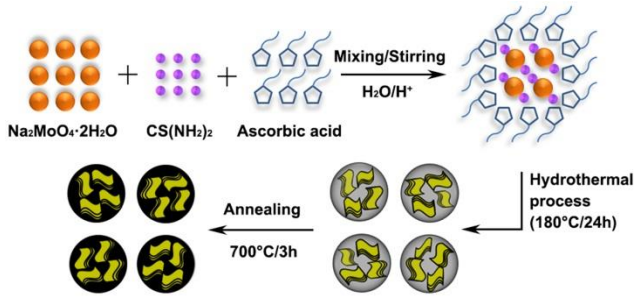

Fig. 1 Schematic illustration of the preparation of MoS_2-C nanocomposites.

X-ray diffraction (XRD) was performed in Rigaku MiniFlex600 using a Cu K_α radiation in the range of $5 - 80°$ at a scanning rate of $4°min^{-1}$. Raman spectra were taken in DXR Thermo-Fisher Scientific with a laser wavelength λ=532 nm. Field-emission scanning electron microscope (SEM) images were taken from JEOL JSM7500F. High resolution transmission electron microscopy (HRTEM) was Philips Tecnai-F20. The carbon content of the MoS_2-C samples was determined by a TG-DSC using NETZSCH, STA 449 F3 with a ramp speed of $5°C\ min^{-1}$ in ambient air in a temperature range of 30 °C to 650 °C.

The electrochemical testing procedure was similar as the previous report.[29] Herein only change is the active materials. The batteries were tested within a potential range of 0.01 - 3 V at various current densities.

3. RESULTS AND DISCUSSION

3.1 Material Characterization. Fig. 2a reveals the TG curves of the MoS_2-C nanocomposites. The mass loss can be attributed to the decomposition of C and MoS_2 in accordance with the following equations:

$$MoS_2 + O_2 \rightarrow MoO_3 + SO_2 \uparrow \quad (1)$$

$$C + O_2 \rightarrow CO_2 \uparrow \quad (2)$$

The decomposition of MoS_2 contributes to the mass loss (Equation (1)), and the carbon content is calculated by Equation (2). The carbon content of the composites are estimated to be 0.4wt%, 2.5wt%, 8.4wt%, and 16.2wt%, Therefore, these samples were labeled as 0.4%C-MoS_2, 2.5%C-MoS_2, 8.4%C-MoS_2 and 16.2%C-MoS_2, respectively.

The X-ray diffraction patterns of the as-prepared 0.4%C-MoS_2, 2.5%C-MoS_2, 8.4%C-MoS_2 and 16.2%C-MoS_2 are shown in the Figure 2b. All the synthesized samples are in accordance with the 2H-MoS_2 (JCPDS card No. 37-1492), yet with weak and broadened peaks. When the content of carbon increases, the peak around 14° ,corresponding to the (002) planes, becomes weaker, which is caused by the breaking of the weak van der Waals force bonds to form disordered layers.[28] Moreover, the peak for the (002) planes shows a slight leftwards shift to a lower angle. Note also that the shift becomes larger as the amount of ascorbic acid rise. Because the (002) planes represent the interlayers of the MoS_2 material, there are inevitable changes to the layer morphology among the as-prepared samples, which could be due to the intercalation of small molecules between the interlayers of MoS_2 after large amounts of carbon coating are applied.[30,31] As shown in Fig. 2c, Raman peaks around 375 cm^{-1} and 405 cm^{-1} correspond to the E_{2g} and A_{1g} vibration modes.[32] According to previous reports, the broadened peaks represent nanoscale morphology,[33] and the shorter peak distance between E_{2g} and A_{1g} also reflects the few-layer structure of the as-prepared samples, especially for the 16.2%C-MoS_2.[13] The carbon coated samples are also characterized in the range from 1100 cm^{-1} to 1800 cm^{-1} (Fig. S1). Compared with 0.4%C-MoS_2 and 2.5%C-MoS_2, the 8.4%C-MoS_2 and 16.2%C-MoS_2 samples show clearer peaks around 1364 cm^{-1} and 1587 cm^{-1}, which are distributed to the D (disordered) band and the G (graphite) band, respectively. The intensity ratio of the D peak to the G peak (I_D/I_G) can reflect the graphitization of each sample. The detailed value of I_D/I_G is 1.05, 0.97, and 0.87

for 2.5%C-MoS_2, 8.4%C-MoS_2 and 16.2%C-MoS_2, respectively. It should be noted that, as the ascorbic acid content increases, the degree of graphitization becomes higher.

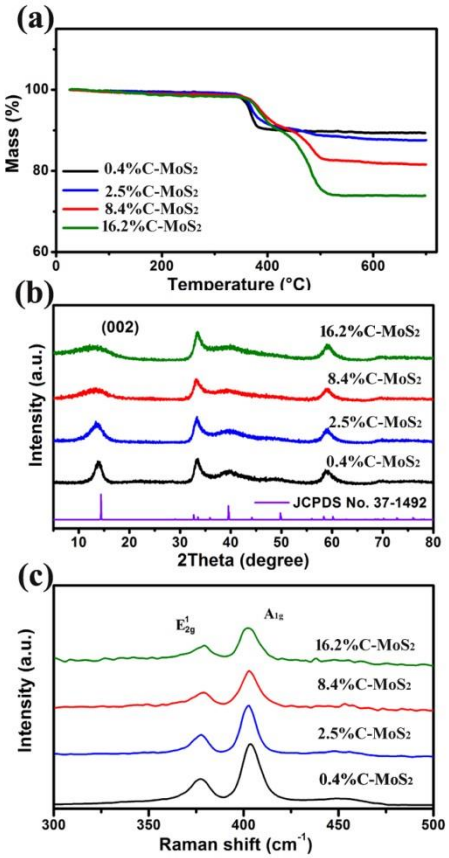

Fig. 2 (a) Thermogravimetric analysis of 0.4%C-MoS_2, 2.5%C-MoS_2, 8.4%C-MoS_2 and 16.2%C-MoS_2 (b) XRD patterns of the as prepared 0.4%C-MoS_2, 2.5%C-MoS_2, 8.4%C-MoS_2 and 16.2%C-MoS_2 (JCPDS No. 37-1492 is served as comparison.) (c) Raman spectra of 0.4%C-MoS_2, 2.5%C-MoS_2, 8.4%C-MoS_2 and 16.2%C-MoS_2 within a range of 300 - 500 cm^{-1}.

Figure 3 presents SEM images of the MoS_2-C samples. With increasing carbon content, the morphology of MoS_2-C changes in three aspects. Firstly, the flower-like morphology partially changes to nanoparticles. The flower-like morphology can be clearly observed for 0.4%C-MoS_2 (Fig. 3a), while a distorted flower-like morphology with sub-microparticles is observed for 2.5%C-MoS_2

(Fig. 3b). The 8.4%C-MoS_2 and 16.2%C-MoS_2 samples did not exhibit a flower-like morphology (Fig. 3c, 3d). Secondly, the size of the nanoparticles is reduced with the increasing carbon content. Compared with the 200 nm particle size of 0.4%C-MoS_2, the particle diameter of 16.2%C-MoS_2 shrinks to 60 nm. Furthermore, the surface area increases. The surface area was found to be 21.47, 47.94, 94.92 and 144.38 m^2g^{-1} for the 0.4%, 2.5%, 8.4%, and 16.2% C samples by the BET method (Fig. S2). The carbon contents thus increase the surface area significantly, and this trend agrees with our previous work.[34]

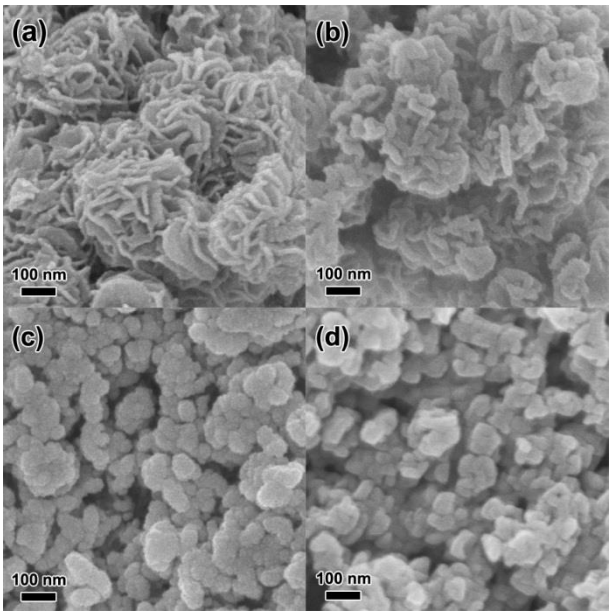

Fig.3 SEM images of (a) 0.4%C-MoS_2, (b) 2.5%C-MoS_2, (c) 8.4%C-MoS_2 and (d) 16.2%C-MoS_2. (All the figures are taken at the same magnification)

Fig. 4 reveals the HRTEM images. From Fig. 4a, the graphene-like MoS_2 with few layers are detected, and no obvious amorphous carbon are found, which means layered construction forms during the hydrothermal process without adding ascorbic acid, and is preserved with less ascorbic acid in the precursors. However, compared to the 0.4%C-MoS_2, the interlayer of 2.5%C-MoS_2 (Fig. 4b) has an expansion from 0.63 nm to 0.66 nm. The carbon layer of 2.5%C-MoS_2 is thinner than that on 8.4%C-MoS_2 and 16.2%C-MoS_2, and cannot be covered the surface completely. The 8.4%C-MoS_2 and 16.2%C-MoS_2 sample display a rather larger layer space of 0.67 nm and 0.70 nm. Furthermore, the surface of 8.4%C-

MoS_2 and 16.2%C-MoS_2 are coated with an amorphous carbon layer (Fig. 4c, 4d). From the HRTEM image of 16.2%C-MoS_2, the carbon layer is much thicker than for the other samples. With increasing carbon content, the MoS_2 layers become distorted, which should be a reasonable explanation for the broadened and weak XRD peak at ~14° for the MoS_2-C nanocomposites. Carbon coating could also help to prevent the restacking of MoS_2, with efficient separation for a few layers of MoS_2 sheets.

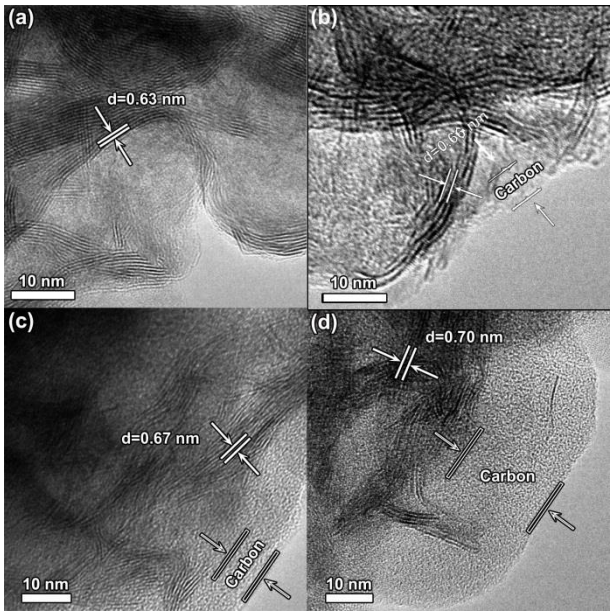

Fig.4 HRTEM images of (a) 0.4%C-MoS_2, (b) 2.5%C-MoS_2, (c) 8.4%C-MoS_2 and (d) 16.2%C-MoS_2.

3.2. Electrochemical Performance. Fig. 5 displays the electrochemical characterization of the as-prepared samples. The specific discharge capacities at the 1st cycle for 0.4%C-MoS_2, 2.5%C-MoS_2, 8.4%C-MoS_2, and 16.2%C-MoS_2 are 887, 822, 1111, and 1297 $mAh \cdot g^{-1}$, and the coulombic efficiencies are 86.1%, 85.2%, 78.9%, and 64.1% at the 1st cycle, respectively. At the 2nd cycle, the discharge capacities become 754, 709, 876, and 893 $mAh \cdot g^{-1}$, respectively. The rate property is presented in Fig. 5a. 8.4%C-MoS_2 achieves a high rate capability, with 970 $mAh \cdot g^{-1}$ at 100 $mA \cdot g^{-1}$ and 710 $mAh \cdot g^{-1}$ at 1000 $mA \cdot g^{-1}$ (after activation). On the contrary, 0.4%C-MoS_2 suffers from rapid capacity fade as the current density increases. 2.5%C-MoS_2 shows improved rate capability

compared to 0.4%C-MoS_2, but the capacity still undergoes a serious decline at high current density. 16.2%C-MoS_2 also features better rate performance, but the electrochemical performance at low current density is worse than that of 8.4%C-MoS_2, which should be ascribed to the carbon content. At a low current density, the Li^+ ion diffusion is hindered by the thicker carbon layers, leading to a low capacity for 16.2%C-MoS_2. 16.2%C-MoS_2 shows better tolerance of higher current densities, owing to the more conductive carbon associated with the higher degree of graphitization. The cycling performance is consistent with the rate performance (Fig. 5b). 8.4%C-MoS_2 and 16.2%C-MoS_2 show better cycling performance, compared to 0.4%C-MoS2 and 2.5%C-MoS_2. 8.4%C-MoS_2 features capacity retention of 97.3% at 100 $mA \cdot g^{-1}$. The charge and discharge curves of the first two cycles at 100 $mA \cdot g^{-1}$ are displayed in Fig. 5c and Fig. S3. 0.4%C-MoS_2 (Fig. S3a) and 2.5%C-MoS_2 (Fig. S3b) show clear discharge platforms. 8.4%C-MoS_2 and 16.2%C-MoS_2 (Fig. S3c), however, do not show any obvious platform, but have a slope instead, which may be owing to the amorphous carbon in the composite resulting in poor crystallinity. And the overlapped voltage range of MoS_2 and carbon also should be taken into account (Fig. S3d). The charge and discharge curves at the 2nd cycle exhibit large changes in the voltage platform, which is very common for the Li_2S/S couple in Li-S batteries.[35-37]

Fig. 5d indicates obvious reduction peaks at 1.06 and 0.59V in the first cycle, corresponding to the formation of Li_xMoS_2 and the decomposition of MoS_2.[18] In the reverse anodic scan, an oxidation peak at 1.57 V corresponds to the partial oxidation of Mo, and another pronounced peak at about 2.3 V is corresponding to S from the oxidation of Li_2S. During the following cycles, these peaks in CV less obvious and the two new reduction peaks at 1.86 V and 1.05 V appear, indicating the formation of Li_2S convert from the S with lithium-ion.[38] Notably, the strength of cathodic peaks weakens rapidly, manifesting an irreversible conversion reaction during the lithium-ion insertion/extraction process. The other samples show the similar tendency with 8.4C%-MoS_2 while suggesting

inferior reversibility (Fig.S4). For the reference, the electrochemical performances of pure carbon are shown in Figure S5. It is declared that pure carbon contributes about 110 mAh g^{-1} at 100 mA g^{-1} after 50 cycles. And the reversible capacity is reduced to 45 mAh g^{-1} at the current density of 400 mA g^{-1}. Considering the theoretical Li-storage capacity of MoS_2 (670 mAh g^{-1}), the theoretical capacity of MoS_2-C at 100 mA g^{-1} is calculated as Equation (3).:

$$C_{8.4\%C\text{-}MoS2} = C_{MoS2} \times \%_{\text{mass of MoS2}} + C_{\text{pure carbon}} \times \%_{\text{mass of pure carbon}} \quad (3)$$

$$= 670 \times 91.6\% + 110 \times 8.4\% = 622.96 \text{ mAh } g^{-1}$$

The high specific capacity of the MoS_2-C (our test result) is attributed not only to flower-like MoS_2 nanosheets, but also to the synergistic effect between the MoS_2 with expanded layers distances and the carbon. Although the reaction mechanism is partly equivalent to Li-S batteries after 1st cycling, the unique large interlayer spacing has still advantageous features as electrodes. MoS_2 nanostructures with a larger spacing result in better material utilization and faster ionic diffusion for the initial lithiation kinetics.[39] Furthermore, according to the galvanostatic charge and discharge profiles of MoS_2-C with the different interlayer space optimized, it shows that the large interlayer space can lower the discharge plateau in favour of applying to the full cells. Moreover, it is claimed that the first intercalation stage is important for optimizing the nanostructured electrode.[40] After the first discharge, full charging–discharging for the Li–MoS_2 system contains intermedium sulfur and the Mo nanoparticles have a multifunctional beneficial effect. First, the particles make for enhancing the electrical conductivity of the Li_2S matrix. Second, the nanoparticles Mo provide adsorption sites for soluble sulfur to prevent their dissolution. Therefore it can relieve the shuttling effect causing performance deterioration and guarantee the stability of cycling. Besides, carbon also works in the above role cooperating with Mo nanoparticles.[41, 42]

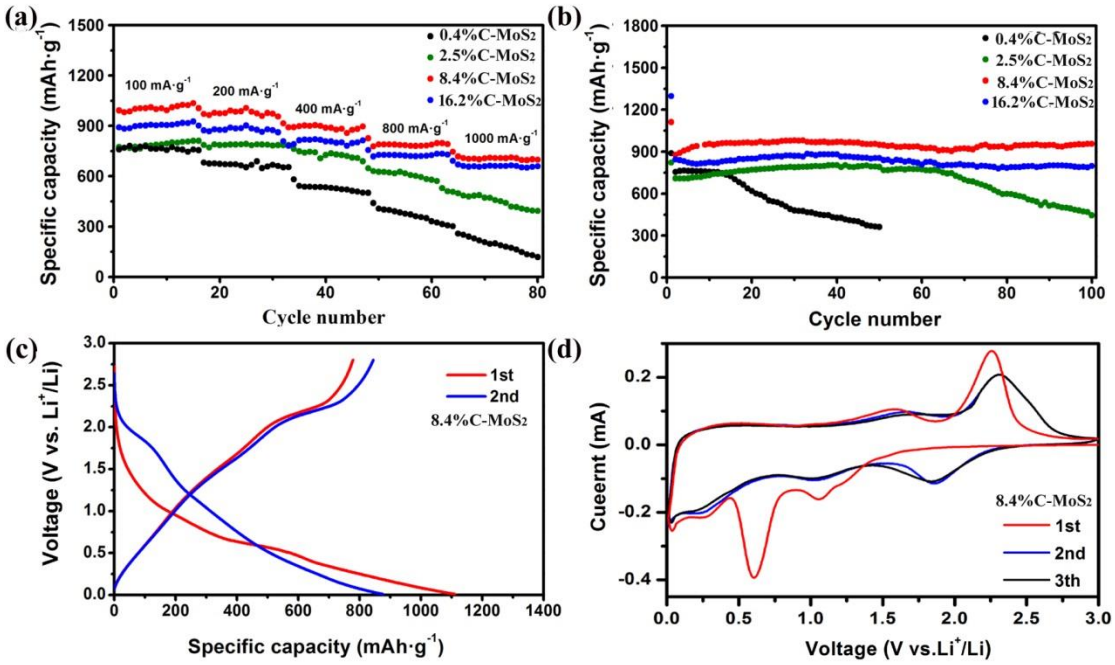

Fig. 5 Electrochemical tests on the MoS_2-C composites. (a) Rate and (b) cycling performances of 0.4%C-MoS_2, 2.5%C-MoS_2, 8.4%C-MoS_2 and 16.2%C-MoS_2. (c) Charge and discharge curves of 8.4%C-MoS_2 at 100mA g^{-1} for the 1st and 2nd cycles, and (d) the initial three CV curves of 8.4%C-MoS_2.

Fig. 6a presents the electrochemical impedance spectra (EIS) of the samples. The signal was collected at 1.0 V in the 1st discharge. The EIS plots consist of a semicircle at high frequency (with the diameter of the semicircle related to the charge transfer resistance) and a line at low frequency (related to the Li^+ ion diffusion). By simulating the EIS data with the equivalent circuit in the inset of Fig. 6a, we have calculated the values of R_{ct} for the samples, and these are shown in Table S1.[43] As the carbon content increases, the value of R_{ct} decreases. The results indicate that 16.2%C-MoS_2 possesses the lowest R_{ct}. EIS characterizations of 2.5%C-MoS_2, 8.4%C-MoS_2, and 16.2%C-MoS_2 after 10, 20, 50 and 100 charge and discharge cycles are shown in Fig. S6. The R_{ct} value of 2.5%C-MoS_2 obviously increases as the charge-discharge cycling proceeds. After 100 cycles, 2.5%C-MoS_2 shows the largest R_{ct} among these three samples. Although the R_{ct} of 16.2%C-MoS_2 after 10 cycles is lower than that of 8.4%C-MoS_2, their R_{ct} values are almost the same after 100 cycles (Table S2). In

particular, the value for 8.4%C-MoS_2 is nearly unchanged after 20 cycles. To understand the in-depth mechanism behind the impedance, the samples were compared using galvanostatic intermittent titration technique (GITT) measured from 0.4 to 3V, based on Fig. S7 and Equation (4).[44] The L is the thickness of the electrode, τ is the titration time, ΔE_s is the difference between two consecutive stabilized open circuit voltage, and D is the variable of Li^+ diffusion coefficients. The battery was discharged at a constant current 0.7 mA for an interval τ of 10 min followed by an open circuit stand for 40 min. The chemical diffusion coefficients of Li^+ are shown in Fig. 6b. It follows that the diffusion coefficients in the MoS_2 composite electrodes are in the range of 10^{-15}-10^{-9} cm^2 s^{-1}. Meanwhile, the diffusion coefficient of 8.4%C-MoS_2 is higher than for the other three nanocomposites from 0.5 V to 1.6 V. This is a convincing clue to the better electrochemical performance of this sample. The above-mentioned electrochemical properties exactly represent the importance of the carbon framework, as in previous work.[45]

$$D = \frac{4}{\pi}\left(\frac{IV_M}{Z_A \mathrm{FS}}\right)^2 \left[\frac{dE(x)}{dx} \Big/ \frac{dE(\tau)}{d\sqrt{\tau}}\right]^2 \qquad \left(\tau \ll \frac{L^2}{D}\right) \qquad (4)$$

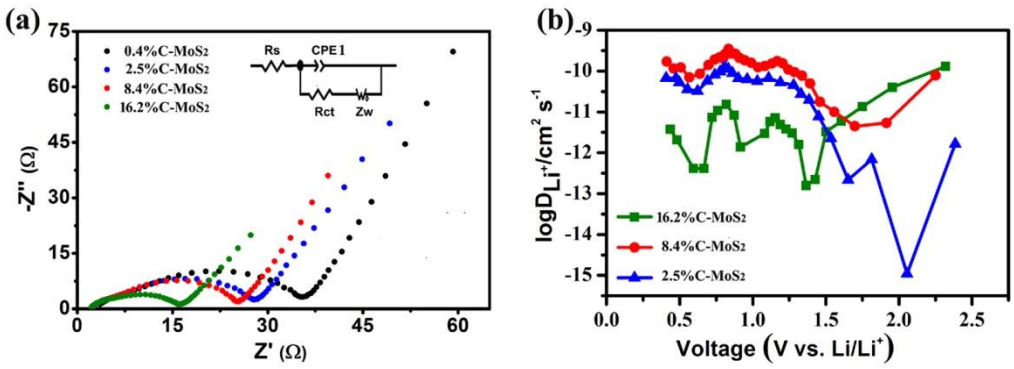

Fig.6 (a) EIS characterization of 0.4%C-MoS_2, 2.5%C-MoS_2, 8.4%C-MoS_2 and 16.2%C-MoS_2 (at the discharge platform of the 1st cycle after activation). The inset is the equivalent circuit (Rs: solution resistance, Rct: charge transfer resistance, Zw: Warburg impedance, CPE1: double layer capacitance between

the electrode and electrolyte.). (b) The chemical diffusion coefficient of Li^+ as a parameter of voltage calculated by GITT.

The excellent electrochemical property of MoS_2-C is ascribed to the following merits. On the one hand, the carbon frame mainly can not only promote the electrons and Li^+ ions diffusion kinetics but also prevent their pulverization and remit the volume expansion of MoS_2. Moreover, the carbon also can serve as conductive material, which avoids the loss of electrochemical contact between the active materials and the current collector, and act as a binder between the Li_2S/S and the Mo nanoparticles.[37] To further explain why 8.4%C-MoS_2 has better electrochemical performance, an ideal model of MoS_2-C nanoparticles with carbon coatings is illustrated in Fig 7. Although the carbon layer restricts the volume change during electrochemical reactions, it also leads to fewer interfaces between MoS_2 and the electrolyte, which means sluggish kinetics and lower specific capacity. For MoS_2 with very little carbon content (Fig. 7a), the MoS_2 surface can't be coated with carbon completely. When the MoS_2 particle is covered by an appropriate carbon content (Fig. 7b), the layer contains randomly distributed defects and vacancies, which promote Li^+ and electron transport.[46] A thick carbon layer on the MoS_2 particle prolongs the distance for Li^+ transport (Fig. 7c). That is the reason why a proper amount of carbon (8.4 wt%) is required in the MoS_2-C composite to give it both high capacity and high rate capability.

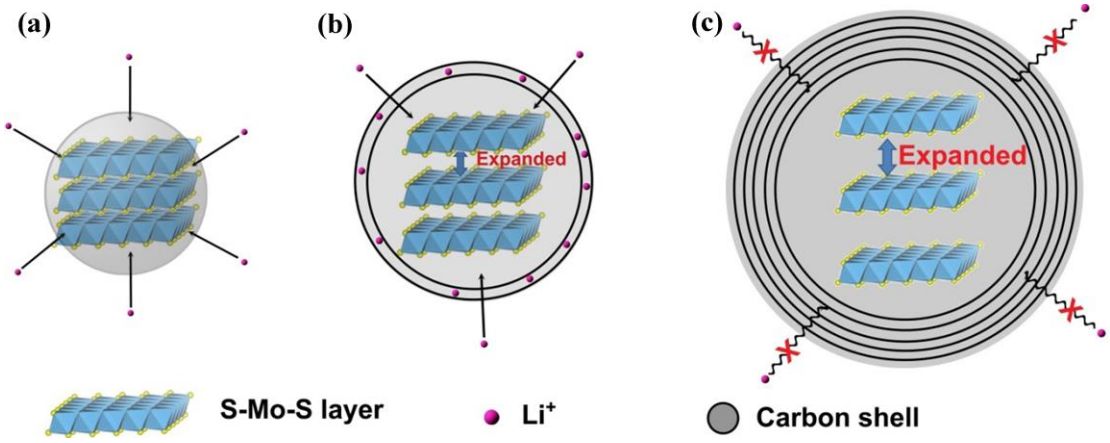

Fig. 7 Proposed models of (a) 2.5%C-MoS_2, (b) 8.4%C-MoS_2, and (c) 16.2%C-MoS_2, showing the effects of the carbon coating layer on the electron conduction and Li^+ transport within the MoS_2-based particles.

4. CONCLUSION

MoS_2-C nanocomposites have been synthesized through an ascorbic-acid-assisted hydrothermal process. Ascorbic acid as a carbon source plays a decisive role in refining the MoS_2 particle size, and enhancing the total electronic conductivity by forming three-dimensional carbon frameworks which not only accelerates the charge transfer kinetics but also guarantees the integrity of the electrode materials. 8.4%C-MoS_2 features the excellent electrochemical performance, due to its optimal carbon content and stable carbon frameworks, and in particular, it is large surface area and many active reactive sites. MoS_2 nanoparticles coated with carbon have great potential for application in rechargeable lithium ion batteries.

ASSOCIATED CONTENT

Supporting Information

The Supporting Information about the detailed description of the experiments is available free of charge on the ACS Publications website

AUTHOR INFORMATION

Corresponding Author

Institute for Superconducting and Electronic Materials, Australian Institute of Innovative Materials, University of Wollongong, Innovation Campus, Squires Way, North Wollongong, NSW 2500, Australia.*Email: shulei@uow.edu.au.

ACKNOWLEDGMENT

This work was supported by the National Natural Science Foundation of China (NSFC 21231005, 51271094), and the 111 Project (B12015). The Australian Research Council has also supported this work through a Linkage Project (LP120200432).

REFERENCES

1 Tarascon, J.-M.; Armand, M. Issues and Challenges Facing Rechargeable Lithium Batteries. *Nature* **2011**, *414*, 359-367.

2 Etacheri, V.; Marom, R.; Elazari R.; Salitra, G.; Aurbach, D. Challenges in the Development of Advanced Li-ion Batteries: A Review *Energy Environ. Sci.* **2011**, *4*, 3243-3262.

3 Shu, H.; Li, F.; Hu, C.; Liang, P.; Cao, D.; Chen, X. The Capacity Fading Mechanism and Improvement of Cycling Stability in MoS_2-based Anode Materials for Lithium-Ion Batteries. *Nanoscale* **2016**, *8*, 2918-2926.

4 Cheng, F.; Liang, J.; Tao, Z.; Chen, J. Functional Materials for Rechargeable Batteries. *Adv. Mater.* **2011,** *23*, 1695-1715.

5 Chhowalla, M.; Shin, H. S.; Eda, G.; Li, L.-J.; Loh, K. P.; Zhang, H. The Chemistry of Two-dimensional Layered Transition Metal Dichalcogenide Nanosheets. *Nature Chem.* **2013**, *5*, 263-275.

6 Lee, Y.; Bae, S.-R.; Park, B. J.; Shin, D. W.; Chung, W. J.; Kang, Y.-M. Sn‐based Chalcogenide Composite as a High‐Capacity Anode Material for Lithium Rechargeable Batteries. *J. Am. Ceram. Soc.* **2012,** *95*, 2272-2276.

7 Zhou, J.; Lan, Y.; Zhang, K.; Xia, G.; Du, J.; Zhu, Y.; Qian, Y. In Situ Growth of Carbon Nanotube Wrapped Si Composites as Anodes for High Performance Lithium Ion Batteries. *Nanoscale* **2016**, *8*, 4903-4907.

8 Zhang, C.; Wang, X.; Liang, Q.; Liu, X.; Weng, Q.; Liu, J.; Yang, Y.; Dai, Z.; Ding, K.; Bando, Y.; Tang, J.; Golberg, D. Amorphous Phosphorus/Nitrogen-Doped Graphene Paper for Ultrastable Sodium-Ion Batteries. *Nano Lett.* **2016**, *16*, 2054-2060.

9 Youn, D.; Heller, A.; Mullins, C. B. Simple Synthesis of Nanostructured Sn/Nitrogen-Doped Carbon Composite Using Nitrilotriacetic Acid as Lithium Ion Battery Anode. *Chem. Mater.* **2016**, *28*, 1343-1347.

10 Du, Y.; Zhu, X.; Si, L.; Li, Y.; Zhou, X.; Bao, J. Improving the Anode Performance of WS_2 through a Self-Assembled Double Carbon Coating. *J. Phys. Chem. C* **2015**, *119*, 15874-15881.

11 Zhou, X.; Wan, L.; Guo, Y. Synthesis of MoS_2 nanosheet-graphene nanosheet hybrid materials for sable lithium storage. *Chem. Commun.* **2013**, *49*, 1838-1840.

12 Cabana, J.; Stoeva, Z.; Titman, J. J.; Gregory, D. H.; Palacín, M. R. Towards New Negative Electrode Materials for Li-Ion Batteries: Electrochemical Properties of LiNiN. *Chem. Mater.* **2008**, *20*, 1676-1678.

13 Li, H.; Wu, J.; Yin, Z.; Zhang, H. Preparation and Applications of Mechanically Exfoliated Single-layer And Multilayer MoS_2 and WSe_2 Nanosheets. *Acc. Chem. Res.* **2014**, *47*, 1067-1075.

14 Wang, Q. H.; Kalantar-Zadeh, K.; Kis, A.; Coleman, J. N.; Strano, M. S. Electronics and Optoelectronics of Two-dimensional Transition Metal Dichalcogenides. *Nature Nanotech.* **2012**, *7*, 699-712.

15 Wan, J.; Bao, W.; Liu, Y.; Dai, J.; Shen, F.; Zhou, L.; Cai, X.; Urban, D.; Li, Y.; Jungjohann, K.; Fuhrer, M. S.; Hu, L. In Situ Investigations of Li‐MoS_2 with Planar Batteries. *Adv. Energy Mater.* **2015,** *5*, DOl: 10. 1002/aenm.201401742.

16 Kong, D.; He, H.; Song, Q.; Wang, B.; Lv, W.; Yang, Q.-H.; Zhi, L. Rational Design of MoS_2@Graphene Nanocables: Towards High Performance Electrode Materials for Lithium Ion Batteries. *Energy Environ. Sci.* **2014**, *7*, 3320-3325.

17 Du, G.; Guo, Z.; Wang, S.; Zeng, R.; Chen, Z.; Liu, H. Superior Stability and High Capacity of Restacked Molybdenum Disulfide as Anode Material for Lithium Ion Batteries. *Chem. Commun.* **2010,** *46*, 1106-1108.

18 Xiong, F.; Cai, Z.; Qu, L.; Zhang, P.; Yuan, Z.; Asare, O. K.; Xu, W.; Lin, C.; Mai, L. Three-Dimensional Crumpled Reduced Graphene Oxide/MoS_2 Nanoflowers: A Stable Anode for Lithium -Ion Batteries. *ACS Appl. Mater. Interfaces* **2015**, *7*, 12625−12630.

19 Chrissafis, K.; Zamani, M.; Kambas, K.; Stoemenos, J.; Economou, N. A.; Samaras, I.; Julien, C. Structural Studies of MoS_2 Intercalated by Lithium. *Mater. Sci. Eng. B* **1989**, *3*, 145-151.

20 Zhu, C.; Mu, X.; van Aken, P. A.; Yu, Y.; Maier J. Single‐Layered Ultrasmall Nanoplates of MoS_2 Embedded in Carbon Nanofibers with Excellent Electrochemical Performance for Lithium and Sodium Storage. *Angew. Chem. Int. Ed.* **2014**, *53*, 2152-2156.

21 Hwang, H.; Kim, H.; Cho, J. MoS_2 Nanoplates Consisting of Disordered Graphene-like Layers for High Rate Lithium Battery Anode Materials. *Nano Lett.* **2011**, *11*, 4826-4830.

22 Zhang, C.; Wang, Z.; Guo, Z.; Lou, X. W. Synthesis of MoS_2–C One-dimensional Nanostructures with Improved Lithium Storage Properties. *ACS Appl. Mater. Inter.* **2012,** *4*, 3765-3768.

23 Zhou, X.; Wan, L.-J.; Guo, Y.-G. Facile Synthesis of MoS_2@ CMK-3 Nanocomposite as an Improved Anode Material for Lithium-ion Batteries. *Nanoscale* **2012**, *4*, 5868-5871.

24 Liu, Y.; Zhao, Y.; Jiao, L.; Chen J. A Graphene-Like MoS_2/Graphene Nanocomposite as a High Performance Anode for Lithium Ion Batteries. *J. Mater. Chem.* **2014**, *2*, 13109-13115.

25 Zhang, N.; Zhao, Q.; Han, X.; Yang, J.; Chen, J. Pitaya-like Sn@ C Nanocomposites as High-rate and Long-life Anode for Lithium-ion Batteries. *Nanoscale*, **2014**, *6*, 2827-2832.

26 Zhang, S.; Yu, X.; Yu, H.; Chen, Y.; Gao, P.; Li, C.; Zhu, C. Growth of Ultrathin MoS_2 Nanosheets with Expanded Spacing of (002) Plane on Carbon Nanotubes for High-Performance Sodium-Ion Battery Anodes. *ACS Appl. Mater. Inter.* **2014**, *6*, 21880-21885.

27 Hu, L.; Ren, Y.; Yang, H.; Xu, Q. Fabrication of 3D Hierarchical MoS_2/Polyaniline and MoS_2/C Architectures for Lithium-ion Battery Applications. *ACS Appl. Mater. Inter.* **2014**, *6*, 14644-14652.

28 Hu, Z.; Wang, L.; Zhang, K.; Wang, J.; Cheng, F.; Tao, Z.; Chen, J. MoS_2 Nanoflowers with Expanded Interlayers as High‐Performance Anodes for Sodium‐Ion Batteries. *Angew. Chem., Int. Ed.* **2014**, *53*, 12794–12798.

29 Hu, Z.; Zhang, K.; Zhu, Z.; Tao, Z.; Chen, J. FeS_2 microspheres with an ether-based electrolyte for high-performance rechargeable lithium batteries. *J. Mater. Chem. A* **2015**, *3*, 12898-12904.

30 Xie, J.; Zhang, J.; Li, S.; Grote, F.; Zhang, X; Zhang, H.; Wang, R.; Lei, Y.; Pan, B.; Xie, Y. Controllable Disorder Engineering in Oxyen-Incorporated MoS_2 Ultrathin Nanosheets for Efficient Hydrogen Evolution. *J. Am. Chem. Soc.* **2013**, *135*, 17881-17888.

31 Hu, X.; Zhang, W.; Liu, X.; Mei, Y.; Huang, Y. Nanostructured Mo-based electrode materials for electrochemical energy storage. *Chem. Soc. Rev.* **2015**, *44*, 2376-2404.

32 Guo, B.; Yu, K.; Li, H.; Song, H.; Zhang, Y.; Lei, X.; Fu, H.; Tan, Y.; Zhu, Z. Hollow Structured Micro/Nano MoS_2 Spheres for High Electrocatalytic Activity Hydrogrn Evolution Reaction. *ACS Appl. Mater. Interfaces* **2016**, *8*, 5517−5525.

33 Tran Khac, B. C.; Jeon, K.-J.; Choi, S. T.; Kim, Y. S.; DelRio, F. W.; Chung, K.-H. Laser-Induced Particle Adsorption on Atomically Thin MoS_2. *ACS Appl. Mater. Interfaces* **2016**, *8*, 2974−2984.

34 Hu, Z.; Zhang, K.; Gao, H.; Duan, W.; Cheng, F.; Liang, J.; Chen, J. Li_2MnSiO_4@C Nanocomposite as a High-Capacity Cathode Material for Li-Ion Batteries. *J. Mater. Chem. A* **2013**, *1*, 12650-12656.

35 Zhang, K.; Zhao, Q.; Tao, Z.; Chen, J. Composite of Sulfur Impregnated In Porous Hollow Carbon Spheres as the Cathode of Li-S Batteries with High Performance. *Nano Res.* **2013**, *6*, 38-46.

36 Xu, G.; Ding, B.; Pan, J.; Nie, P.; Shen, L.; Zhang, X. High Performance Lithium–Sulfur Batteries: Advances and Challenges. *J. Mater. Chem. A* **2014**, *2*, 12662-12676.

37 Ji, X.; Lee, K. T.; Nazar, L. F. A Highly Ordered Nanostructured Carbon–Sulphur Cathode for Lithium–Sulphur Batteries. *Nat. Mater.* **2009**, *8*, 500-506.

38 Hu, S.; Chen, W.; Zhou, J.; Yin, F.; Uchaker, E.; Zhang, Q.; Cao, G. Preparation of Carton Coated MoS_2 Flower-like Nanostructure with Self-assembled Nanosheets as High-performance Lithium-ion Battery Anode. *J. Mater. Chem. A* **2014**, *2*, 7862-7872.

39 Xiao, J.; Choi, D.; Cosimbescu, L.; Koech, P.; Liu, J.; Lemmon, J. P. Exfoliated MoS2 Nanocomposites as an Anode Material for Lithium Ion Batteries. *Chem. Mater.* **2010**, *22*, 4522-4524.

40 Xu, X.; Liu, W.; Kim, Y.; Cho, J. Nanostructured Transtion Metal Sulfides for Lithium Ion Batteries: Progress and challenges *Nano Today* **2014**, *9*, 604-630.

41 Ji, X.; Lee, K. T.; Nazar, L. F. A Highly Ordered Nanostructured Carbon-sulphur Cathode for lithium-sulphur batteries. *Nature Materials* **2009**, *8*, 500-506.

42 Zhang, B.; Qin, X.; Li, G. R.; Gao, X. P. Enhancement of Long Stability of Sulfur Cathode by Encapsulation Sulfur into Micropores of Carbon Spheres. *Energy Environ. Sci.* **2010**, *3*, 1531-1537.

43 Chang, K.; Chen, W. L-Cysteine-Assisted Synthesis of Layered MoS_2/Graphene Composites with Excellent Electrochemical Performances for Lithium Ion Batteries. *ACS Nano* **2011**, *5*, 4720-4728.

44 Zheng, W.; Shui, M.; Shu, J.; Gao, S.; Xu, D.; Chen, L.; Feng, L.; Ren, Y. GITT Studies on Oxide Cathode $LiNi_{1/3}Co_{1/3}Mn_{1/3}O_2$ Synthesized by Citric Acid Assisted High-Energy Ball Milling. *Bull. Mater. Sci.* **2013**, *36*, 495-498.

45 Hu, S.; Chen, W.; Zhou, J.; Yin, F.; Uchaker E.; Zhang Q.; Cao G.; Preparation of Carbon Coated MoS_2 Flower-Like Nanostructure with Self-assembled Nanosheets as High-Performance Lithium-ion Battery Anodes. *J. Mater. Chem. A* **2014**, *2*, 7862-7872.

46 Zhu, Z.; Cheng, F.; Chen, J. Investigation of Effects of Carbon Coating on the Electrochemical Performance of $Li_4Ti_5O_{12}$/C Nanocomposites. *J. Mater. Chem. A*, **2013**, *1*, 9484-9490.

Table of Contents Graphic